Journal of Computer-Aided Molecular Design, **16:** 27–41, 2002.
KLUWER/ESCOM

Molecular docking studies of a group of hydroxamate inhibitors with gelatinase-A by molecular dynamics

Tingjun Hou, Wei Zhang & Xiaojie Xu*
College of Chemistry and Molecular Engineering, Peking University, Beijing 100871, P.R. China

Received 17 July 2001; Accepted 7 February 2002

Key words: gelatinase-A, MMP-2, hydroxamate, molecular dynamics, molecular docking

Summary

We have performed docking and molecular dynamics simulations of hydroxamates complexed with human gelatinase-A (MMP-2) to gain insight into the structural and energetic preferences of these inhibitors. The study was conducted on a selected set of eleven compounds with variation in structure and activity. Molecular dynamics simulations were performed at 300 K for 100 ps with equilibration for 50 ps. The structural analyses of the trajectories indicate that the coordinate bond interactions, the hydrogen bond interactions, the van der Waals interactions as well as the hydrophobic interactions between ligand and receptor are responsible simultaneously for the preference of inhibition and potency. The ligand hydroxamate group is coordinated to the catalytic zinc ion and form stable hydrogen bonds with the carbonyl oxygen of Gly 162. The P1′ group makes extensive van der Waals and hydrophobic contacts with the nonpolar side chains of several residues in the S1′ subsite, including Leu 197, Val 198, Leu 218 and Tyr 223. Moreover, four to eight hydrogen bonds between hydroxamates and MMP-2 are formed to stabilize the inhibitors in the active site. Compared with the P2′ and P3′ groups, the P1′ groups of inhibitors are oriented regularly, which is produced by the restrain of the S1′ subsite. From the relationship between the length of the nonpolar P1′ group and the biological activity, we confirm that MMP-2 has a pocket-like S1′ subsite, not a channel-like S1′ subsite proposed by Kiyama (Kiyama, R. et al., J. Med. Chem. 42 (1999), 1723). The energetic analyses show that the experimental binding free energies can be well correlated with the interactions between the inhibitors and their environments, which could be used as a simple score function to evaluate the binding affinities for other similar hydroxamates. The validity of the force field parameters and the MD simulations can be fully testified by the satisfactory agreements between the experimental structure-activity relationship and the information from the structural and energetic analyses. The information generated from the predicted complexes should be useful for further work in the area of structure-based design of new compounds.

Introduction

Matrix metalloproteinases (MMPs) are a class of structurally related enzymes that are responsible for the metabolism of extracellular matrix proteins [1–3]. These zinc and calcium dependent enzymes are synthesized as zymogens and under physiological conditions the proteins are selectively regulated by inhibitors called tissue inhibitors of Metalloproteinases (TIMPS) [4, 5]. The extracellular matrix functions as a medium of migration, attachment, and structural support in various cell types and tissues. Therefore, MMPs play a crucial role in matrix remodeling events of connective tissues during embryonic growth and wound healing [6–8]. Increased activity of the MMPs has been associated with a wide range of pathological diseases such as arthritis, cancer, multiple sclerosis and Alzheimer's disease [9–10]. Hence, the molecular-level insights obtained on MMP inhibition in this study will have an impact on the future rational design of MMP inhibitors that could be useful in the treatment of the disease states described above.

*To whom correspondence should be addressed.
E-mail: xiaojxu@chem.pku.edu.cn.

On the basis of substrate specificity and primary sequence similarities, the members of the matrixin family can be grouped into five subfamilies: gelatinases (MMP-2, -9), which cleave denatured collagen, elastin, and type IV and V collagens; collagenases (MMP-1, -8, -13), which cleave triple-helical interstitial collagen; stromelysins (MMP-3, -10, -11), which mainly cleave proteoglycans; membrane-type MMPs (MMP-14, -15, -16, -17), which are associated with activation of pro-MMPs; and others (MMP-7, etc) [6, 11] At the molecular level, MMPs are characterized by a zinc atom at the active site (zinc catalytic site) with a conserved zinc binding motif, HExxHxxGxxH. The proenzyme region also contains a cysteine residue which is conserved in MMPs, and in the inactive form this cystine is bonded to the catalytic zinc. This class of enzyme also contains a methionine residue below the active site zinc, which forms part of a family-wide superimposable 'Met-turn' [12–13].

Since MMPs are involved in a wide range of diseases, there has been interest in obtaining effective small-molecule inhibitors. Recently, a number of pseudo-peptide inhibitors have been reported in the literature [14]. Generally speaking, the requirement for a molecule to be an effective inhibitor of the MMP class of enzymes is a functional group (e.g., hydroxamic acid, carboxylic acid, and sulfhydryl, etc.) capable of attaching to the catalytic zinc atom, at least one functional group which provides a hydrogen bond interaction with the enzyme backbond, and one or more side chains which undergo effective van der Waals interactions with the enzyme subsites. Moreover, some inhibitors can demonstrate binding affinities to several MMPs, which can be naturally deduced that the binding modes between different inhibitor and different MMP are somewhat similar. Of all these inhibitors, compounds with the hydroxamate zinc binding group may be the most popular ones in MMPs such as MMP-1, MMP-2, MMP-3 and MMP-9 etc. The crystal structures of hydroxamate inhibitors complexed with MMPs have revealed that the catalytic zinc is pentacoordinated with three histidine nitrogens in MMP-2 and two hydroxamte oxygens in inhibitor (see Figure 1) [15].

Among the subfamilies of MMPs, gelatinases have been considered to be very promising for use in drug development. Since gelatinases are thought to play an important role in triggering the processes of tumor growth, invasion and metastasis by cleaving the vascular basement membrane which consists of type IV collagen, gelatinase inhibitors have been studies

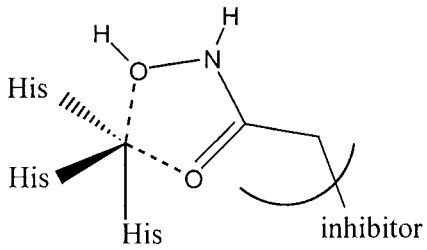

Figure 1. The catalytic zinc atom coordinated by thee liganding histidine nitrogens of the enzyme and both hydroxamate oxygens.

extensively in the search of a new type of anticancer drug [16–18]. The resolution of the crystal structure of MMP-2 gave the opportunity to develop new compounds by the structure-based approach [19]. But until now, X-ray structures of the MMP-2-inhibitor complexes have not been reported, and the theoretical studies on the binding mode of the MMP2 with its inhibitors were essentially necessary, which can provide insights into the interaction occuring in the active site. In this paper, eleven hydroxamtes with wide range of binding affinities to MMP-2 were selected for molecular docking and dynamics simulations.

Computational methods

All the MD simulations were done with AMBER 6.0 molecular simulation package [21]. An AMBER force field was used for molecular minimizations and dynamics. The analysis of MD trajectories was performed using AMBER 6.0 and in-house software. Quantum mechanical calculations were carried out using Mopac 7.0 and Gaussian 98 [22, 23]. All the calculations were performed on a 2-CPU SGI Octane workstation and a home-made Linux parallel computing system with 22 Pentium PIII733 CPUs. Visualization and molecular construction were performed using the Insight II and Sybyl 6.7 molecular simulation package [24, 25].

The initial structures of hydroxamates complexed with MMP-2

Starting enzyme structure of MMP-2 (PDB entry 1qib) was obtained from the Protein Data Bank [19]. All the hydrogens were added and enzyme structure was subjected to a refinement protocol in which the constraints on the enzyme were gradually removed. The energy minimizations were carried out using AMBER program until the rms gradient was smaller than

Table 1. Structures of the studied hydroxamate inhibitors and experimental binding free energies for MMP-2.

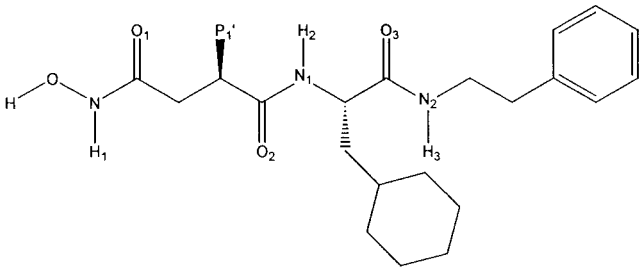

No.	R^1	ΔG (kcal/mol)
A1	CH_2Ph	-7.80
A2	$(CH_2)_2Ph$	-11.80
A3	$(CH_2)_3Ph$	-13.92
A4	$(CH_2)_4Ph$	-13.09
A5	$(CH_2)_3C_6H_{11}$	-11.13
A6	$(CH_2)_3$Ph-4Me	-13.77
A7	$(CH_2)_3$Ph-4OMe	-13.93
A8	$(CH_2)_3$Ph-4F	-13.93
A9	$(CH_2)_3$Ph-4Et	-13.28

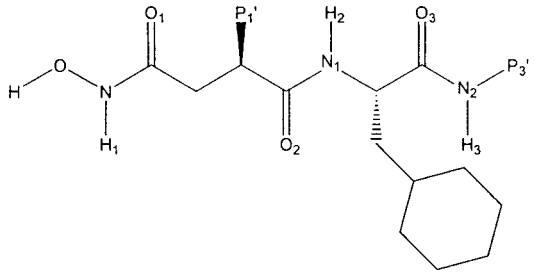

No.	P_1'	P_3'	ΔG (kcal/mol)
A10	$(CH2)_3$Ph-4Cl	$(CH_2)_2CO_2H$	-15.01
A11	$(CH2)_3$Ph-4Cl	$(CH_2)_2CO_2Me$	-15.01

0.05 kcal/mol. During the refinement process, all heavy atoms were restrained to their positions after minimizations with 10 kcal/mol/Å^2 harmonic forces. The energy-minimized structure was used for docking studies. A series of MMP-2 inhibitors belonging to the class the hydroxamates were selected for the present study [26]. Enzyme inhibitory activity in terms of experimental binding free energies, ΔG_b, are reported in Table 1.

The X-ray crystal of proMMP-3 with a hydroxamate inhibitor (PDB entry 1biw) obtained by Natchus et al. was treated as the template molecule to construct the complexes of MMP-2 with hydroxamates [27]. The catalytic domain of the MMP-2 is similar to that of proMMP-3. The same residues form the substrate binding pockets and coordination of the catalytic Zn^{2+} ion is quite similar. Also, the binding site for the structural Zn^{2+} ion is identical to a well-conserved motif found in all known MMP structures. So we believe that the constructed complexes of MMP-2 with hydroxamates from the crystal structure of a proMMP-3 complex are precise enough as the initial structures for MD simulations. First, MMP-2 and MMP-3 were superimposed by structural alignment. Then, the hydroxamate inhibitor was extracted from 1biw and merged into 1qib. Last, each compound was

docked into the active site by modifying the crystal structure ligand as a template for the initial placement. During this model-building process, the conformation of the protein was not altered, and the inhibitor structures were altered minimally to avoid unacceptable atom bump.

Force field

Most bond and angle parameters associated with the zinc center were taken from Hoops et al. [28] All the torsions associated with the zinc-ligand bonds were set to zero as in Hoops et al. Three angle parameters concerned with the zinc center, absent from the work of Hoops et al., were taken from the studies of Ryde [29]. These three angles include C-O-Zn, CV-NB-Zn and HO-OH-Zn. The force field parameters associated with N-O functionality for the studied molecules were taken from Taba et al. [30] Some missing parameters concerned with inhibitors were obtained from the newest AMBER force field (parm99) revised by Wang et al. [31]. In Wang's work, some parameters especially for small molecules, absent in the previous AMBER force field, were developed [32]. All force field parameters for the zinc ion and the hydroxamate group associated with MMP inhibitors were shown in Table 2. In this paper, all atoms are represented with the atom types defined in the AMBER force field.

The potentials of the structural and catalytic zinc centers were represented with the nonbonded and bonded approaches, respectively. We believe that the structural zinc do not directly influence the ligand binding, and the conformation near the structural zinc can be maintained using nonbonded interaction combined with a structural restrain. Three calcium ions in 1qib were also represented with nonbonded approach. So formal charges of $+2|e|$ were assigned to the structural zinc and three calcium ions. The charge representations of the catalytic zinc ion were obtained by the two ESP fitting calculations adopted in our previous work [33]. In the first stage, the partial charges on the zinc ion were determined by using a simplified active site model. The structure shown in Figure 2 was adopted as the theoretic model for the complex structure of MMP-2 and inhibitors at the active site. The simplified model only include the zinc ion, three histidines and the inhibitor coordinated. In this model, acetohydroxamate ($CH_3C(O)NHOH$) was used as a simplified inhibitor. H atoms were substituted at N-terminal residues and hydroxy groups were substituted at carbonyl groups at C-terminal residues.

Table 2. Derived force field parameters for the zinc ions and some groups associated with MMP inhibitors.

Bond parameters		
Bond	K_r (kcal/Å^2)	R_{eq} (Å)
Zn-NB	40.0	2.05
Zn-OH	40.0	2.20
Zn-O	40.0	2.05
N-O	539.0	1.37

Angle parameters		
Angle	K_θ (kcal/rad^2)	θ_{eq} (degree)
NB-Zn-NB	20.0	105.0
NB-Zn-O	20.0	115.0
CR-Zn-NB	20.0	126.0
N-OH-HO	83.6	105.6
OH-N-C	137.4	116.1
H-N-OH	94.8	109.1
C-O-Zn	24.0	131.2
CV-NB-Zn	20.0	126.0
HO-OH-Zn	28.9	110.3

Dihedral parameters			
Dihedral	ν (kcal/mol)	γ (degree)	*n*
HO-OH-N-C	6.0	180	1

The resulting geometry was fully optimized by using the AM1 Hamiltonian in MOPAC 7.0 before performing a single-point *ab initio* calculations with no further geometry optimization. The Hartree-Fock method with the 6-31G* basis set applied in the Gaussian 98 program was used to determine electrostatic potentials. Finally, the partial charges were derived using the Restrained Electrostatic Potential (RESP) fitting method provided by AMBER [34]. In this stage, the partial charges for the catalytic zinc, three liganding histidines and two hydroxamate oxygens were determined. In the second stage, the partial charges of the studied inhibitors were obtained. All the molecules shown in Table 1 modified from the hydroxamate in 1BIW were fully minimized by the AM1 Hamiltonian in MOPAC 7.0. The Hartree-Fock method with the 6-31G* basis set applied in the Gaussian 98 program were used to determine electrostatic potentials. RESP fitting technique in AMBER was applied to determine the partial charges. Because of the absence of the crystal structures of the complexes, we could not explicitly

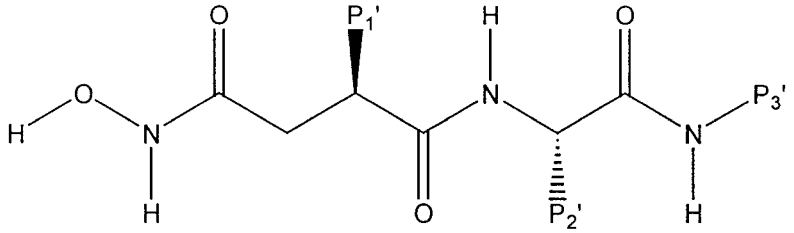

Figure 2. The common structure of the hydroxamate inhibitor.

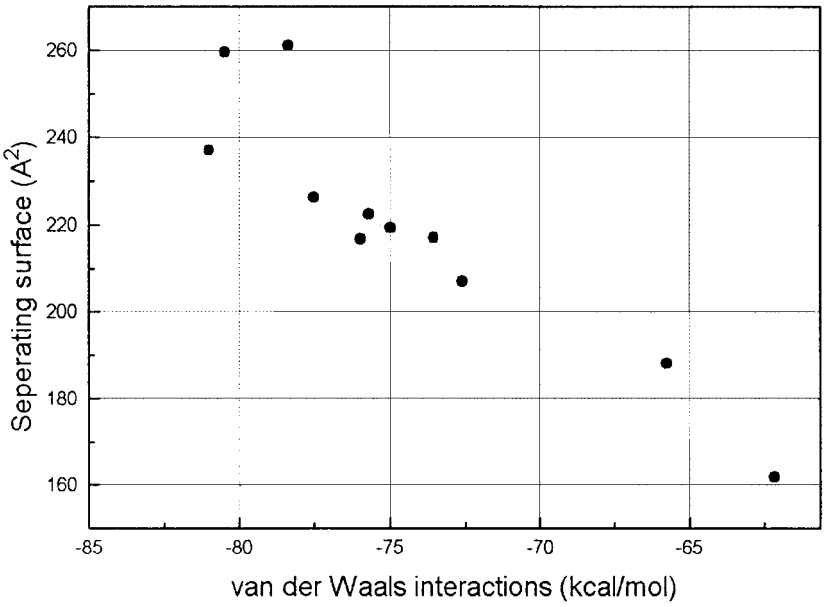

Figure 3. The relationships between van der Waals interaction and the separating surfaces.

consider the influence of environment to the inhibitors during the determination of partial charges. We believe that when the hydroxamates in Table 1 are recognized by MMP-2, the partial charges on two hydroxamate oxygens would be quite similar to those on two hydroxamate oxygens in acetohydroxamate. So during the ESP calculations, two Lagrange constrains in RESP were used to fix the partial charges on the O and O1 atoms to those values from the first stage, while the partial charges on the other atoms were determined from the ESP fitting.

MD simulations

All MD simulations were performed using AMBER 6.0. The charges resulted from the ESP calculations were incorporated into the AMBER force field. From the calculated results, the partial charges on three histidines coordinated with catalytic zinc ion are quite different, meanwhile, they are significantly different from the standard AMBER values, so we need to make some modifications to the AMBER database file and PDB file to properly recognize those three different residues. In AMBER, we defined thee kinds of new residues: HIA, HIB and HIC, and they represented His 201, His 205 and His 211 in 1qib, respectively. The partial charges on these three newly defined residues were revised from the default values in AMBER to the ESP charges in this paper. Moreover, we defined a new zinc unit to represent the catalytic zinc center. Each ligand studied was defined as a new type of residue and added to the AMBER database files. All force field parameters in Table 1 were added to the AMBER force field file.

MD simulations were carried out at 300 K. A explicit solvent model TIP3P water was used. The complex was solvated with a 20 Å water cap from the center of mass of the ligands. Prior to MD simulations, a series of minimization were carried out using a protocal in which all heavy atoms were restrained with 1,000, 1000, and 10 kcal/mol/Å^2 harmonic forces re-

spectively. Subsequently, a cycle of minimization was done to relax all the atoms without constraints. The maximum number of minimization steps was 20,000 steps and the convergence criterion for the energy gradient was 0.05 kcal/mol/Å. Then, MD simulation procedure for the solvated enzyme-inhibitor complex involved (1) 50 ps of MD simulations for equilibrium, (2) 100 ps of MD simulations for data collection. In the data collection stage, every 200 fs, the snapshot was recorded into a trajectory file. In MD simulations, all residues within 16 Å were allowed to move, while the others were restrained by a 50 kcal/mol/Å harmonic force. The SHAKE procedure was employed to constrain all bonds involving at least one hydrogen atom. The time step of the simulations was 2.0 fs with a cutoff 12 Å for the nonbonded interactions. The nonbonded pairs were updated every 30 steps.

Results and discussion

Almost all ligands contain the hydrophobic side chains on P1′ and P2′ substituent sites (see Figure 2), respectively. The P1′ group of the inhibitors is in the protein interior, whereas the P2′ group is solvent-exposed. Most of the effective ligands have a hydrophobic group in the P1′ position (e.g., the CH_2Ph, $(CH2)_3Ph$ groups et al.) and take advantage of the favorable van der Waals and hydrophobic interactions provided by the S1′ subsite of MMPs. Hydrophilic interactions such as hydrogen bonds between the inhibitors and enzyme also significantly contribute to ligand binding.

Representative stereplots of the inhibitors and some residue directly concerned with ligand binding are shown in Figure 4–8. The illustrations are taken from the 100 ps MD data collection stage in the averaging runs. All hydrogen atoms and water molecules have been removed for clarity.

The hydroxamate zinc binding group

Table 3 shows the distances of bonds between ligand and catalytic zinc ions. It is obvious that the coordination of the inhibitor's hydroxamate group to the catalytic zinc atom was maintained very well for the entire simulation time, which can be suggested by the low rms fluctuations of these five coordinate bonds (note that these distance were not constrained by SHAKE). For the available crystal complex structures of MMPs, the hydroxamate zinc binding group acts as a bidentate ligand with each oxygen (O and O1) situated at an optimum distance (1.9–2.3 Å) from the catalytic zinc ion. From our simulations, we can see that both oxygens at O and O1 position retain their stable ligand interaction with the catalytic zinc ion (Table 3) within the region from the crystal structures. Moreover, the zinc ion remains pentacoordinated form with the two hydroxamate oxygens and the three histidine nitrogens in the active site. Furthermore, a stable hydrogen bond can be observed between O atom of ligand and the backbond carbonyl oxygen of Gly 162 (In this paper, all atoms are represented with the atom name defined in the AMBER residue database file). All simulated results above suggest that the hydroxamate zinc binding group is one of the primary determinant as in the case of other zinc-binding groups, such as a carboxylate group, for binding of the studied inhibitors.

The interactions between the P1′ groups and the S1′ subsite

All compounds in Table 1 have a hydrophobic substituent in the P1′ position. In fact, most of the effective MMP inhibitors have a nonpolar substituent in the P1′ position and take advantage of the favorable van der Waals interactions provide by the nonpolar atoms in the active site.

To inhibitors A1 to A9, besides the P1′ groups, the other structures of them are completely same. But their binding affinities are quite different, so it is naturally deduced that the interaction between the P1′ group and the S1′ subsite plays a crucial role in inhibitor-enzyme recognition process. We think that the influences of the different P1′ groups may be interpreted by using the steric complementarity and the van der Waals interactions.

In the current work, we used the principle of the separating surface area (*SSA*) to measure the steric complemtarity between the P1′ group and the S1′ subsite. This method was proposed by Keil et al. in 1998 [35]. The separating surface is defined by a set of points located halfway on the shortest distance vectors between surface points of the two molecular partners. The surface is generated using a grid-based algorithm. The distance to the nearest atom is stored on the grid points and an isosurface is generated forming the separating surface. Size and shape of the surface characterises the complex interface. In our paper, the separating surfaces between the P_1' groups of hydroxamates and the S1′ subsite of MMP-2 were modeled by using the MOLCAD module in Sybyl 6.5 molecular simulations package. The calculated results show that the separating surfaces are determined by the size

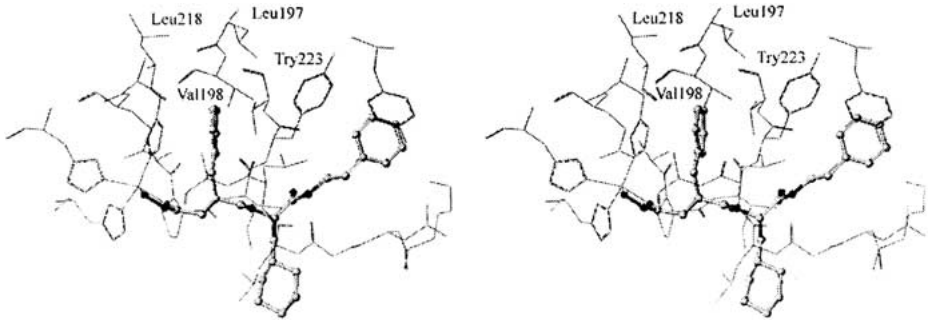

Figure 4. Steroplot of the binding site for complex of A1 with MMP-2 from the average conformation of the MD simulations. Only residues within 4 Å of any atom of the inhibitor are shown in Figure 6–10.

Table 3. Selected metal–ligand distance calculated from the MD trajectories[a,b].

	O[c]	O1[c]	NE2 His 201	NE2 His 205	NE2 His 211
A1	2.099 (0.087)	2.266 (0.086)	2.088 (0.083)	2.178 (0.079)	1.997 (0.087)
A2	2.130 (0.085)	2.271 (0.084)	2.047 (0.086)	2.226 (0.082)	2.007 (0.084)
A3	2.041 (0.083)	2.308 (0.080)	1.967 (0.083)	2.176 (0.081)	1.969 (0.083)
A4	2.110 (0.084)	2.253 (0.083)	2.071 (0.085)	2.205 (0.084)	2.011 (0.080)
A5	1.981 (0.088)	2.338 (0.082)	1.944 (0.084)	2.088 (0.080)	1.994 (0.088)
A6	2.072 (0.087)	2.269 (0.087)	2.024 (0.087)	2.169 (0.084)	1.983 (0.081)
A7	2.099 (0.081)	2.287 (0.086)	2.066 (0.082)	2.161 (0.083)	2.012 (0.089)
A8	2.117 (0.086)	2.269 (0.086)	2.078 (0.079)	2.177 (0.076)	2.000 (0.086)
A9	2.091 (0.083)	2.284 (0.085)	2.050 (0.076)	2.185 (0.076)	2.017 (0.083)
A10	2.114 (0.081)	2.248 (0.089)	2.207 (0.083)	2.218 (0.072)	1.984 (0.088)
A11	2.087 (0.084)	2.281 (0.085)	2.025 (0.087)	2.203 (0.084)	2.014 (0.085)
Mean	2.086 (0.040)	2.279 (0.024)	2.050 (0.066)	2.182 (0.035)	1.999 (0.015)

[a]Results averaged over 100 ps of MD trajectories.
[b]The rms fluctuations are given in parentheses.
[c]O and O1 represent O and O1 in ligands.

of the P1′ groups. Since the complex interface between the P1′ groups and MMP-2 are constituted by nonpolar atoms, the van der Waals interactions between ligand and MMP-2 should exist some relationships with the steric complementarity. Figure 3 shows the relationships between the van der Waals interactions and the separating surfaces. It is interesting to find that the van der Waals interactions between inhibitors and MMP-2 are nearly linearly correlated with the separating surfaces. The strong dependence between the van der Waals interactions and the seperating surfaces demonstrates that the van der Waals interactions between inhibitors and MMP-2 are dominated by the contact sufaces between the P1′ groups and the S1′ subsite.

In order to get more detailed picture about the residues in the active site contacting with the inhibitors, we performed more detailed analysis to investigate the interface between the P1′ groups and the S1′ subsite. Here, we defined a concept of '*interface residue*', which means the residues directly contacting with the inhibitors. We used the solvent-accessible surface area (*SASA*) proposed by Lee and Richards to determine the characteristics of residues in the complex interface [36]. An approach of two-stage surface calculations was adopted to determine the interior interface residue. For a complex, its *SASA* was calculated twice: once for the complex and the other for the uncomplexed MMP-2. From the two-stage *ASA* analysis, we got the polar and nonpolar ratio of the interface for the hydroxmates/MMP-2 complexes. Since the characteristics of the surface complementarity between MMP-2 and all the hydroxamates studied here should be quite similar, we only carefully studied the complex systems of MMP-2 with A3 as a case study. Table 4 shows the total area, polar area and nonpolar area of these residues in the complex interface. From the sum of the polar and nonpolar areas of these residues, it can be found that the sum of the nonpo-

Table 4. The total, polar and nonpolar area of the residues in the **A3**/MMP-2 complex interface.

	Total (Å^2)	Polar (Å^2)	Nonpolar (Å^2)
Leu 197	9.246	2.862	6.444
Val 198	11.867	0.000	11.867
Ala 217	2.102	2.102	0.000
Leu 218	12.056	4.903	7.153
Ala 220	2.110	2.110	0.000
Tyr 223	64.957	9.325	55.632
Thr 224	10.593	8.197	2.396
Sum	112.931	29.499	83.492

lar area (83.492 Å^2) is much larger than that of the polar one (29.499 Å^2). Therefore, the nonpolar S1′ pocket can produce strong van der Waals interactions with the nonpolar P1′ groups in the inhibitors. Moreover, the calculated results indicate there are seven interface residues in the S1′ subsite, while their areas in the interface bear some differences. Among these seven residues, two residues including Ala 217 and Ala 220 seem not important, because their total interface areas are very small. The contacting atoms of Thr 224 with ligands are polar dominated, and this residue seems not helpful to enhance the ligand binding. The residue Tyr 223 may be the most important contributor to the van der Waals interactions between ligand and enzyme, because its nonpolar interface area is much larger than the other ones. From the analyses of the interface of MMP-2 and A3, it is obvious that four residues including Leu 197, Val 198, Leu 218 and Tyr 223 may be the most important residues responsible for ligand binding in the S1′ subsite. In spatial distribution, these four residues are neighboring, which can constitute a relatively large nonpolar and hydrophobic environment. Moreover, from the MD trajectory for the MMP-2/A3 complex, it can be found that the benzene rings of the inhibitor and Tyr 223 prefer to be parallel. The distance between their mass centers of those two benzene rings is about 4 Å–5 Å, and we believe that the pair parallel benzene rings may produce relatively strong aromatic stacking interactions.

There was a significant amount of movement of the inhibitors in the active site during the simulations, but in all cases it was confined primarily to the P'_2 and P'_3 groups of the inhibitors. We can treat the inhibitors in the average complex from the MD trajectories as the active compounds. We aligned these active inhibitors using atom-by-atom least-square fit implemented in the 'SYBYL FIT' option in SYBYL. Figure 9 shows the aligned inhibitors from the average conformation of the MD trajectories. From Figure 9, we can find that the orientation of the P1′, P2′ and P3′ groups are quite different. The P1′ groups for all these 11 inhibitors possess very specific orientations. The benzene rings in the P1′ groups for 10 inhibitors exhibit parallel states. The channel-like S1′ pocket make the P1′ groups to adopt specific orientation. But to the P2′ and P3′ groups, they do not show regular orientation (see Figure 11). It seems that there do not exist strong and specific interactions between MMP-2 and the P2′ or P3′ groups to limit their movement. So it seems that the variations of the P2′ and P3′ groups may not introduce signficant effect to the binding free energies, because they are partly solvent-exposed and only introduce limited influence to the conformation of the inhibitors.

Hydrogen bond interactions between hydroxamates and MMP-2

The analyses of the MD trajectories show that all the studied inhibitors can form several stable hydrogen bonds with the protein. All the protein-inhibitor backbone hydrogen can be well maintained throughout the simulations. So the hydrogen bonds between hydroxamates and MMP-2 are also critical to ligand binding. In the current wok, we carefully investigated these hydrogen bonds from the MD trajectories. All analysis was performed using the *carnal* program in AMBER. All investigated protein-inhibitor backbone hydrogen bonds and their average distances from the MD trajectories are listed in Table 5. Table 5 shows that there are totally twelve hydrogen bonds concerned with seven residues. We find that the frequencies of these hydrogen bonds are quite different. Some hydrogen bonds are present in most complexes, while some hydrogen bonds are only available in one or two systems. So from the frequencies of the hydrogen bonds, the hydrogen bonds can be divided into two categories: the conserved hydrogen bonds and the nonconservative ones. The conserved hydrogen bonds include five hydrogen bonds: the hydroxamte O atom with the carbonyl oxygen (O) of GLY 162, the hydroxamate N atom with the O2 atom of Leu 164, the hydroxamte N atom with the carboxylate oxygen (OE2) of Glu202, the hydroxamate N1 atom of the carbonyl oxygen (O) of Pro221 and the hydroxamate O3 atom with the N atom of Tyr223, which can be found at least in eight complexes. The other seven hydrogen bonds

Table 5. The Distance of hydrogen-bonds between inhibitors and protein from the MD trajectories.

No.	1	2	3	4	5	6
Inhibitor	O	N	O2	N	N1	O3
Protein	O GLY 162	O2 LEU 164	N ALA 165	OE2 GLU 202	O PRO 221	N TYR 223
A1	2.839 (0.115)	3.361 (0.321)		2.811 (0.136)		
A2	2.918 (0.156)			3.231 (0.157)	3.710 (0.283)	2.923 (0.150)
A3	3.030 (0.186)	3.758 (0.226)		2.819 (0.279)	3.391 (0.276)	2.886 (0.276)
A4		3.082 (0.166)			3.265 (0.224)	
A5	2.890 (0.133)	3.843 (0.430)		2.784 (0.121)	3.130 (0.216)	2.951 (0.142)
A6	3.362 (0.713)	2.876 (0.122)		2.779 (0.117)	3.263 (0.268)	2.836 (0.103)
A7	2.931 (0.150)	2.930 (0.133)	3.643 (0.235)	2.747 (0.089)	3.278 (0.230)	2.911 (0.123)
A8		2.876 (0.105)		2.773 (0.093)	3.430 (0.283)	2.869 (0.109)
A9		2.937 (0.129)		2.778 (0.100)	2.946 (0.141)	2.870 (0.118)
A10	2.812 (0.138)	2.838 (0.102)		2.825 (0.134)	2.894 (0.119)	2.987 (0.174)
A11	2.872 (0.115)	3.301 (0.246)		2.989 (0.235)		2.918 (0.133)

No.	7	8	9	10	11	12
Inhibitor	N	O3	O1	O1	O4	O4
Protein	OE1 GLU 202	N LEU 163	OE1 GLU 202	OE2 GLU 202	N GLY 162	OD1 ASP 161
A1						
A2						
A3						
A4		3.127 (0.222)	3.127 (0.222)	2.616 (0.096)		
A5						
A6	3.986 (0.314)					
A7	3.886 (0.216)					
A8						
A9						
A10	3.466 (0.234)				3.619 (0.559)	2.952 (0.341)
A11					3.291 (0.265)	

are considered as nonconservative ones, because they can only be found in less than four systems. We think that the residues concerned with the conserved hydrogen bonds are more common and important for ligand binding, and they possess more opportunities to produce strong hydrogen bond interactions with inhibitors.

Structure-activity relationships

The tendency of the biological activities from the inhibitors in Table 1 can be successfully explained by the changes of the van der Waals interactions and hydrogen bond interactions. For example, the hydroxamates A1 to A3 show a clear stepwise increase in MMP-2 binding affinities according to the straight elongation of the P1′ group. In viewing the structure for the A1/MMP-2 complex (Figure 4), it is obvious that the nonpolar P1′ group is in only close contact with the hydrophobic side chain of Val 198 and Tyr 223. The relatively short P1′ group of A1 can not move into the interior of the S1′ subsite and produce good steric complementarity. The separating surface of A1 with MMP-2 is only 188.19 $Å^2$, which is smaller than those of the other inhibitors with MMP-2. When the replacement of the CH_2Ph with $(CH_2)_2Ph$ of A2, the binding affinities is promoted significantly. This SAR is accounted for by significant improvement of the separating surface (207.07 $Å^2$) and van der Waals interactions (-72.61 kcal/mol) of the longer P1′ group with MMP-2. When the P1′ group is $(CH_2)_3Ph$, the steric interaction between A3 and MMP-2 will be optimal, which is revealed by the large separating surface (237.14 $Å^2$). From Figure 5, we find that the P1′

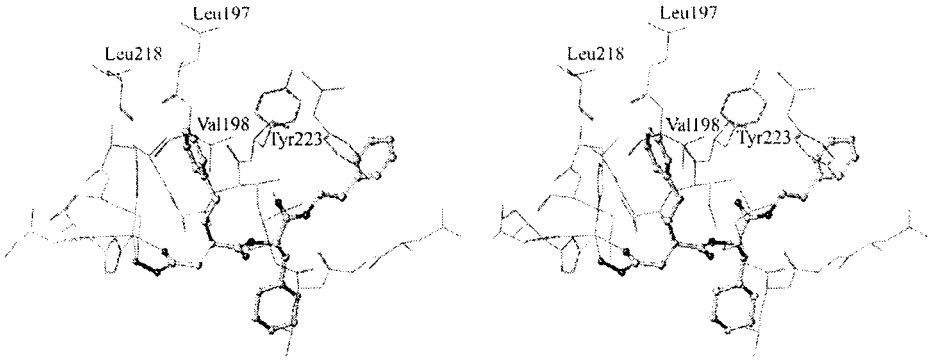

Figure 5. Steroplot of the binding site for complex of A2 with MMP-2 from the average conformation of the MD simulations.

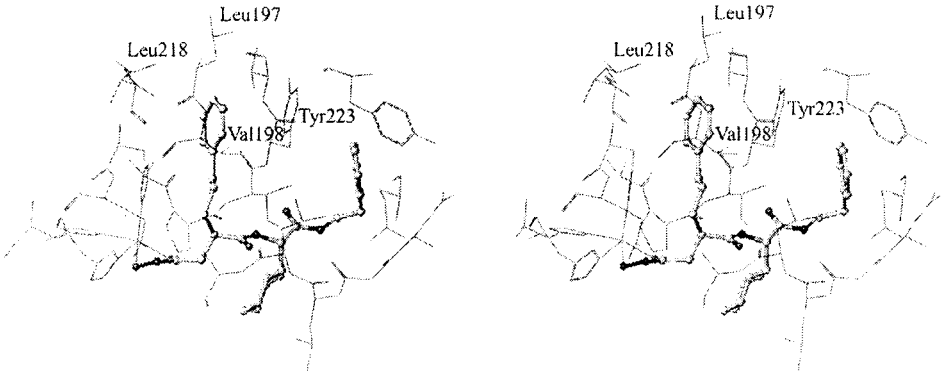

Figure 6. Steroplot of the binding site for complex of A3 with MMP-2 from the average conformation of the MD simulations.

group ($(CH_2)_3Ph$) are fully capped by the S1′ subsite consisting of the side chains of four residues nearby, including Leu 197, Val 198, Leu 218 and Tyr 223. Among compounds A1 to A4, compound A1 is the most inactive one, and it can only produce three stable hydrogen bonds with some polar atoms in MMP-2, including O atom of Gly 162, O2 atom of Leu 164 and OE1 atom of Glu 202. Compound A2 is more active than A1, and it can produce four stable hydrogen bonds with MMP-2. Compound A3 are more active than A2, and it can produce five hydrogen bonds with MMP-2.

But when P1′ of A3 is elongated of P1′ by one CH_2 to $(CH_2)_4Ph$, the free binding energy of A4 is decreased. Compared with the inhibitor A3, the separating surface (237.14 $Å^2$) and the van der Waals (-81.01 kcal/mol) interaction between A4 and MMP-2 are improved (see Table 6). Only from the analysis of van der Waals, the binding capability of A4 should be stronger than that of A3. So, the decease of the binding free energy of A4 should come from the unfavorable electrostatic interaction and coordinating bonding energy. Table 6 shows that the electrostatic interaction (-51.48 kcal/mol) and coordinating bonding energy (28.94 kcal/mol) of A4 with its environments are really weaker than those of A3 with its environment. Because the volume of the P1′ group of A4 is larger than that of A3, if the P1′ group of A4 are fully buried in the S1′ pocket, bad van der Waals contact between A4 and MMP-2 should be produced. In order to produce the best steric complementarity between A4 with MMP-2, some part of the P1′ group of A4 will move outside the S1′ subsite, and some hydrogen bonds and coordinate bonds between MMP-2 and A4 will be weakened (Figure 4).

Among all the studied inhibitors, compounds A10 and A11 possess the strongest binding affinities, besides the favorable van der Waals contacts between the P1′ groups and the S1′ pocket, the formation of additional hydrogen bonds are also important. Both of A11 and A12 possess a carboxy group, and these two oxygen atoms of this group can generate two additional hydrogen bonds with O atom of Pro 221 and N atom of Tyr 223.

The molecular docking and dynamics simulations for hydroxmates with MMP-2 have resulted in a deep

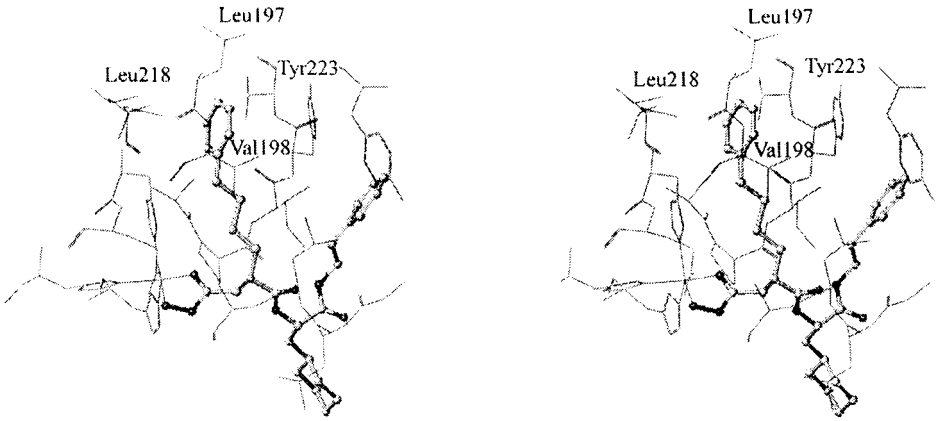

Figure 7. Steroplot of the binding site for complex of A4 with MMP-2 from the average conformation of the MD simulations.

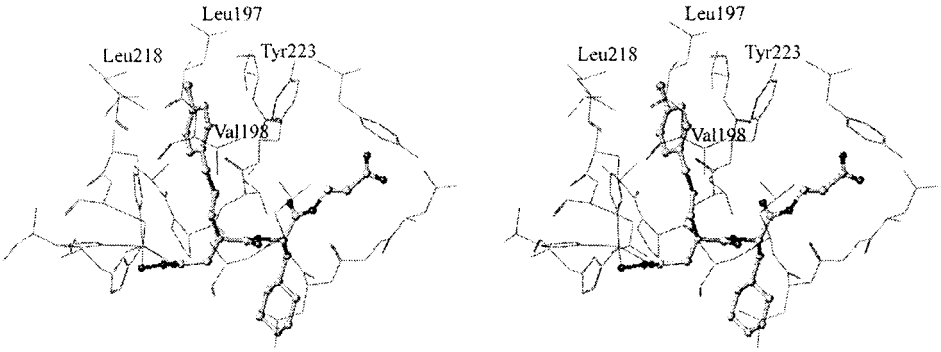

Figure 8. Steroplot of the binding site for complex of A10 with MMP-2 from the average conformation of the MD simulations.

insight into the factors responsible for their inhibition and potency. A schematic representation of all the interactions between these compounds and MMP-2 is presented in Figure 10. In Figure 10, only the conserved hydrogen bonds are represented.

From the MD trajectories, we can get the average nonbonded interactions between the inhibitors and their environments (including MMP-2 and solvent). Table 6 shows the averaged nonbonded interaction and the corresponding energetic components (including the bonded interaction concerned with the coordinated bonds, the electrostatic interaction and the van der Waals interaction). In the MD simulations, the AMBER force field from Cornell et al. was used. The parameters in this all-atom force field omit the hydrogen bonding terms of earlier, so no separate hydrogen bonding energy is shown in Table 6. From the energetic values, we find that the information from the above structural analyses can be well correspondent with that from the energetic analyses. From the structural analyses, we have known that to the compounds A1 to A3, the steric complementarity of the P1′ group of A1 with MMP-2 is the worst, while that of the P1′ group of A3 with MMP-2 is the best. So, the inhibitor A3 prefers to form more favorable van der Waals interactions with the protein. Table 6 clearly demonstrates that the van der Waals interactions between A3 and its environment is -72.61 kcal/mol, which is more favorable than that between A2 and environment (-65.75 kcal/mol). While the van der Waals interaction between A1 and environment is the weakest, which is -62.17 kcal/mol. The P1′ group of A4 is longer than that of A3, but the binding affinity of A4 is weaker than that of A3. So the longer p1′ group of A4 may affect the coordinate bonds and the hydrogen bonds between A4 and MMP-2. Table 6 indicates that the van der Waals interaction between A4 and environment is favorable, but the bonded interaction (28.94 kcal/mol) and the electrostatic interaction (-52.48 kcal/mol) become weaker. The combined effects of these three kinds of interactions make the binding free energy of A4 weaker than that of A3, but stronger than that of A2. The structural analyses have validated that the carboxy group of A10 is

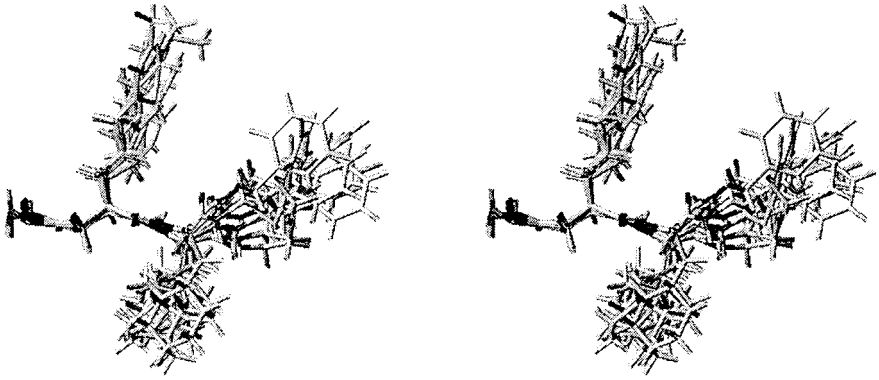

Figure 9. Steroplot of the aligned inhibitors from the average conformation of the MD trajectories.

Table 6. Calculated interactions between the inhibitors and their environments.

No.	E_{total} (kcal/mol)	E_{vdw} (kcal/mol)	E_{elec} (kcal/mol)	E_{coor} (kcal/mol)
A1	−93.28	−62.17	−55.30	24.19
A2	−102.86	−65.75	−63.44	26.33
A3	−109.94	−72.61	−56.63	19.31
A4	−104.55	−81.01	−52.48	28.94
A5	−101.92	−75.99	−51.91	25.98
A6	−106.95	−77.53	−54.52	25.10
A7	−113.65	−80.47	−58.11	24.93
A8	−108.04	−74.99	−55.71	22.66
A9	−113.41	−78.36	−55.25	20.20
A10	−120.99	−73.56	−67.75	20.32
A11	−109.78	−75.71	−56.39	22.33

very important. One carboxy oxygen can form two hydrogen bonds with the O atom of Pro221 and the N atom of Tyr223. The calculated electrostatic interaction between A10 and MMP-2 (−67.75 kcal/mol) is really the lowest, which is more favorable than those between the other inhibitors and MMP-2.

Figure 11 shows the linear relationship of interactions between the studied hydroxamates and their environments *vs* experimental binding free energies. It is obvious that binding free energies are closely correlated with the interactions between the inhibitors and their environments, which is indicated by the high correlation coefficient of the linear model ($r = 0.867$). Certainly, the interactions between the inhibitors and their environments are quite different from the binding free energies, because many factors did not be considered, for example, the desolvation energy and the entropic effects. Considering the similarity of the studied molecules, the contributions of the desolvation energy and the entropic effects to the binding free energy may not exist large differences. So the variation of the experimental ligand binding can be quantitatively predicted based on the interactions between the inhibitors and their environments from the energetic analyses. This theoretical model is quite simple, but it verifies the validity of the molecular docking simulations, the bonded approach and the force field parameters for the catalytic zinc ion. In fact in many docking procedures, the simple nonbonded interactions between ligand and enzyme are often treated as the score function to evaluate binding affinities [37–38].

The bottom shape of the S1′ subsite in MMP-2

Finally, we want to discuss one problem about the bottom shape of the S1′ subsite in MMP-2. In previous work of Kiyama et al., [34], the authors confirmed that MMP-9 had a pocket-like S1′ subsite with a floorboard and MMP-2 had a channel-like S1′ subsite. In his work, the author synthesized some inhibitors hav-

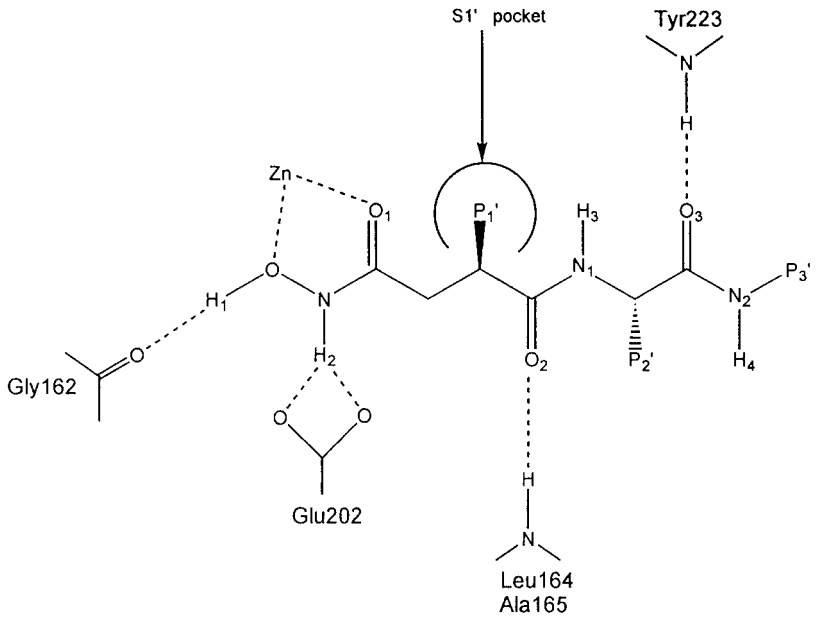

Figure 10. Schematic representation of the interaction model observed in the MD simulations of inhibitor bound to MMP-2.

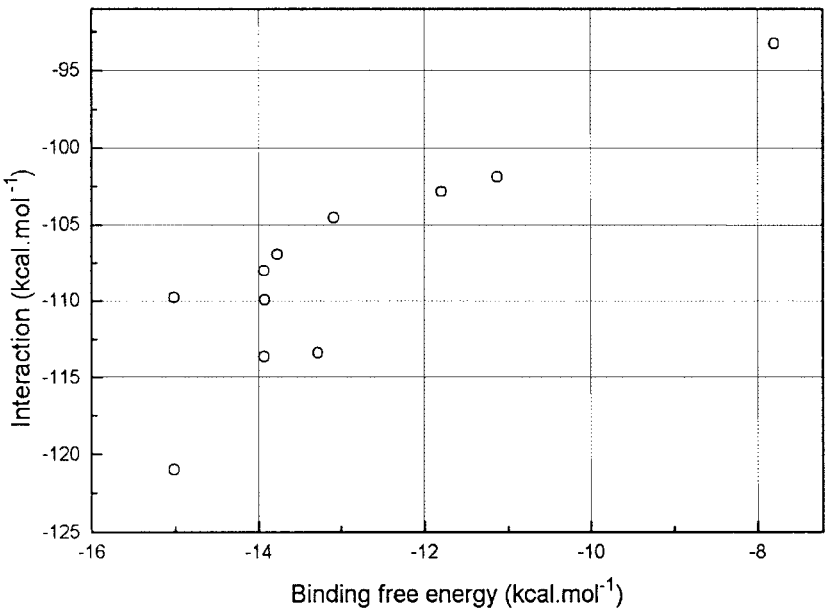

Figure 11. The relationship between the binding free energies and the calculated interactions between ligand and environment.

ing an elongated hydrophobic subsituents in the P1′ position and measured their inhibitory potency against MMP-9 and MMP-2. From the results of molecular docking simulations, they found that those compounds with long P1′ group could protrude from the S1′ subsite channel. So, the authors confirmed that MMP-2 had a channel-like subsite. But our simulations and the previous experiments give a different result. Our simulations clearly demonstrate that when the length of the P1′ group is increased to some extent, the further elongation of the P1′ group will be unfavorable to the binding of the inhibitors. Moreover, the structures of the predicted complexes shows that the bottom of the S1′ subsite are not open. So, the unfavorable van der Waals interactions make the P1′ groups of the inhibitors very difficult to protrude from the bottom of

the S1′ subsite. In the Kiyama's work, the author used a MMP-2 structure from the homology modeling. We know that several residues in the S1′ subsite belong to the loop regions, which are not highly conserved. The homology modeling may not produce the accurate conformation for the S1′ loop. We think that the different docking results may mainly come from the different starting structures used in the current work and Kiyama's work.

Conclusion

By using the MD simulations and the three-dimensional structure of MMP-2, we have succeeded in obtaining reasonable binding model that are, at least qualitatively, consistent with the structure-activity data of eleven compounds. In the current work, a bonded model for the catalytic zinc center was used to represent the bonded interactions between zinc center and enzyme/inhibitor. The point charges for catalytic zinc center, the hydroxamates and three histidines coordinated to zinc atom were determined using a two stage ESP fitting calculations. In the obtained complex structures, the coordination of the inhibitor's hydroxamate group to the catalytic zinc atom was maintained, moreover, in MD simulations the zinc ion remained pentacoordinated with the two oxygens and the three histidines in the active site. The P1′ groups of the hydroxamates interact with Leu197, Val 198, Leu218 and Tyr223, which can generate favorable van der Waals contacts and hydrophobic interactions. If the P1′ groups have suitable length, the phenyl ring in ligand and that in Tyr223 may produce relatively strong aromatic stacking interactions. The MD simulations reveal that the hydrogen bond interactions between ligand and enzyme are also very important for tight binding. Several hydrogen bonds concerned with five residues, including Gly162, Leu164, Glu202, Pro221 and Tyr223, are conserved in most predicted complexes.

From the energetic analyses, we found that the experimental binding affinities could be well linearly related with the nonbonded interaction between ligand and environment. The simple theoretical model can be treated as the relatively accurate score function to evaluate the new inhibitors with unknown binding free energies.

X-ray analysis of the complex is essential for very accurate study, but the validity of the predicted complexes in this paper can be well verified by the satisfactory agreement between the structural analyses and the energetic analyses from the MD trajectories. The structural information from the predicted complex is very important for us to gain insight into the potential mechanisms of the intermolecular interactions between inhibitor and receptor, especially with respect to the design of new compounds.

Acknowledgements

We are particularly grateful to P.A. Kollman and J.M. Wang of University of California San Francisco for their free distributions of the newest Amber force field and giving us helps in MD simulations. This project is supported by NCSF 29992590-2 and 29573095.

References

1. Woessner, J.F., FASBE J., 5 (1991) 2145.
2. Nagase, H. and Fields, G.B., Biopolymer, 40 (1996) 399.
3. Bottomley, K.M.K., Bradshaw, D. and Nixon, J.S., Metalloproteinases as Targets for Anti-Inflammatory Drugs. Birkhäuser Verlag, Switzerland, 1999.
4. Willenbrock F., Murphy G., Am. J. Resp. Crit. Car. Med., 150 (1994) 5165.
5. Green, J., Wang, M., Liu, Y.E., Raymond, L.A., Rosen, C., Shi, Y.E., J. Biol. Chem., 271 (1996) 30375.
6. Murphy, G.J.P., Murphy, G., Reynolds, J.J., FEBS Lett., 289 (1991) 4.
7. Cossins, J., Dudgeon, T.J., Catlin, G., Gearing, A.J.H., Clements, J.M., Biochim. Biophys. Res. Commun., 228 (1996) 494.
8. Pendás, A.M., Knäuper, V., Puente, X.S., Llano, E., Mattei, M.G., Apte, S., Murphy, G., López-Otín, C., J. Biol. Chem., 272 (1997) 4281.
9. Birkedal-Hansen, H., Moore, W.G., Bodden, M.K., Windsor, L.J., Birkedal-Hansen, B., DeCarlo, A, Engler, J.A., Crit. Rev. Oral. Biol. Med., 4 (1993) 197.
10. Coussens, L.M., Werb, Z., Chem. Biol., 3 (1996) 895.
11. Muller, D., Quantin, B., Gesnel, M.C., Millon-Collard, R., Abecossis, J., Breathnach, R., Biochem. J., 253 (1988) 187.
12. Bode, W., Gomis-Rüth, F.X, Stöcher, W., FEBS Lett., 331 (1993) 134.
13. Stöcker, W., Grams, F., Baumann, U., Reinemer, P., Gomis-Rüth, F.X., Mckay, D.B., Bode, W., Protein Sci., 4 (1995) 823.
14. Whittaker, M., Floyd, C.D., Brown, P., Gearing, A.J.H., Chem. Rev., 99 (1999) 2735.
15. Spurlino, J.C., Smallwood, A.M., Carlton, D.D., Banks, T.M., Vavra, K.J., Johnson, J.S., Cook, E.R., Falvo, J., Wahl, R.C., Pulvino, T.A., Wendoloski, J.J., Smith, D.L., Proteins: Struct., Funct., and Genet., 19 (1994) 98.
16. Liotta, L.A., Steeg, P.S., Stetler-Stevenson, W.G., Cell, 64 (1991) 327.
17. Stetler-Stevenson, W.G., Aznavoorian, S., Liotta, L.A., Annu. Rev. Cell. Biol., 9 (1993) 541.
18. Beckett, R.P., Davidson, A.H., Drummond, A.H., Drug Discov. Today, 1 (1996) 16.

19. Dhanaraj, V.W., Ye, Q.Z., Molina, F., Johnson, L.L., Ortwine, D.F., Pavlovsky, A., Rubin, J.R., Skeean, R.W., White, A.D., Humblet, C., Hupe, D.J, Blundell, T.L., Croatica Chemica Acta, 72 (1999) 575.
20. Morgunova, E., Tuuttila, A., Bergmann, U. Isupov, M., Lindqvist, Y., Schneider, G., Tryggvason, K., Science, 284 (1999) 1667.
21. Case, D.A., Pearlman, D.A., Caldwell, J.W., Cheatham, III, T.E., Ross, W.S., Simmerling, C.L., Darden, T.A., Merz, K.M., Stanton, R.V., Cheng, A.L., Vincent, J.J., Crowley, M., Tsui, V., Radmer, R.J., Duan, Y., Pitera, J., Massova, I., Seibel, G.L., Singh, U.C., Weiner, P.K., Kollman P.A. AMBER 6. University of California, San Francisco, 1999.
22. MOPAC 7.0 User Guide, Quantum Chemistry Program Exchange (QCPE), Indiana University, USA, 1993.
23. Gaussian 98 User Guide, Gaussian, Inc., Pittsburgh, USA, 1998.
24. InsightII User Guide, Molecular simulations Inc., San Diego, USA, 1999.
25. SYBYL, version 6.5, Tripos Associates: St. Louis, MO, USA, 1999.
26. Poter, J.R., Beeley, N.R.A., Boyce, B.A., Bioorg. Med. Chem. Lett., 4 (1994) 2741.
27. Natchus, M.G., Cheng, M.Y., Wahl, C.T., Bioorg. Med. Chem. Lett., 8 (1998) 2077.
28. Hoops, S.C., Anderson, K.W., Merz, K.M., Jr., J. Am. Chem. Soc., 113 (1991) 8262.
29. Ryde, U., Proteins: Struct., Funct., and Genet, 21 (1995) 40.
30. Toba, S., Damodaran, K.V., Merz, K.M. Jr., J. Med. Chem., 42 (1999) 1225.
31. Wang, J.M., Cieplak, P., Kollman, P.A., J. Comput. Chem., 21 (2000) 1049.
32. Cornell, W.D., Cieplak, P., Bayly, C.I., Gould, I.R., Merz, K.M., Ferguson, D.M., Spellmeyer, D.C., Fox, T., Caldwell, J.W., Kollman, P.A., J. Am. Chem. Soc., 117 (1995) 5179.
33. Hou, T.J., Zhang, W., Xu, X.J.J., Phys. Chem., 105 (2001) 5304.
34. Cleplak, P., Cornell, W.D., Bayly, C., Kollman, P.A., J. Comput. Chem., 16 (1994) 1357.
35. Keil, M., Exner, T., Brickmann, J., J. Mol. Model., 4 (1998) 335.
36. Lee, B., Richards, F.M., J. Mol. Biol., 55 (1971) 379.
37. Hou, T.J., Wang, J.M., Chen L.R., Xu, X.J., Protein Eng., 12 (1999) 639.
38. Meng, E.C., Shoichet, B.K., Kuntz, I.D.J., Comput. Chem., 13 (1992) 505.
39. Kiyama, R., Tamura, Y., Watanabe, F., Tsuzuki, H., Ohtani, M., Yodo, M., J. Med. Chem., 42 (1999) 1723.